



Nanostructured titanium alloys and multicomponent bioactive films: Mechanical behavior at indentation

E.A. Levashov^{a,*}, M.I. Petrzhik^a, D.V. Shtansky^a, Ph.V. Kiryukhantsev-Korneev^a, A.N. Sheveyko^a, R.Z. Valiev^b, D.V. Gunderov^b, S.D. Prokoshkin^a, A.V. Korotitskiy^a, A.Yu. Smolin^c

^a National University of Science and Technology MISIS, Leninsky pr. 4, Moscow 119049, Russia

^b Institute for Physics of Advanced Materials, Ufa State Aviation Technical University, ul. K. Marx 12, Ufa 450000, Russia

^c Institute of Strength Physics and Materials Science, Siberian Branch, Russian Academy of Sciences, Tomsk 634050, Russia

ARTICLE INFO

Article history:

Received 15 May 2012

Received in revised form

15 January 2013

Accepted 16 January 2013

Available online 31 January 2013

Keywords:

Equal channel angular processing

Thermomechanical processing

Nanostructured titanium alloys and coating

Nanoindentation

Localized deformation

Mechanical behavior

ABSTRACT

Structure and mechanical properties of nanostructured Ti and Ti–Ni, Ti–Nb–Zr, Ti–Nb–Ta shape memory alloys, and TiCaPCON biocompatible coatings were characterized by metallographic analysis and instrumented indentation. Discussed is the mechanism of localized deformation of the coatings deposited onto nanostructured substrates. Deformation was found to proceed inhomogeneous, through formation of shear bands during penetration of a Vickers diamond indenter into TiCaPCON coatings on the substrates with high elastic modulus especially.

© 2013 Elsevier B.V. All rights reserved.

1. Introduction

Wide use of metallic implants in medicine (traumatology, orthopedics, and stomatology) gives impetus to a search for and development of new biocompatible materials with elevated strength and low elasticity modulus close to that of bone tissue. Nowadays, a main implant material is commercially pure titanium [1] which exhibits good biocompatibility. However, the ultimate tensile strength (UTS) and yield stress ($\sigma_{0.2}$) of Ti Grade 4 (worldwide strongest brand) do not exceed 760 and 650 MPa, respectively. Meanwhile, the mechanical properties of metals and alloys can be drastically improved upon a decrease in their mean grain size (d_{gr}) down to 100 nm by using the methods of severe plastic deformation (SPD) [2]. Thus prepared nanostructured (hereinafter, ns) titanium with elevated strength and biocompatibility was suggested as a promising material for implant applications [3]. A process for fabricating ns-Ti ($d_{gr} \approx 150$ nm, UTS > 1250 MPa) was developed at the Ufa State Aviation Technical University (USATU) [4,5]. It involves the CONFORM processing yielding ns-Ti followed by drawing into cylindrical rods 6 mm in diameter and up to 3 m long [4,5]. The process has been implemented at the innovative enterprise NanoMet Ltd. (Ufa, Russia).

Other promising candidate materials under consideration are shape memory alloys (SMAs). Their medical applications revealed [6–9] a number of their functionalities that cannot be achieved with conventional materials and technologies. In order to improve service parameters of the above alloys, of current interest seemed to be the preparation of ns-SMAs via thermomechanical treatment (TMT). Most suitable functional properties (recovery strain, recovery stress, superelastic deformation) combined with optimal mechanical properties and corrosion resistance are exhibited by Ti–Ni-based SMAs (titanium nickelide, NITINOL) [6–10].

However, medical applications of NITINOL are restricted by the presence of toxic Ni in this alloy. This circumstance gave start to extensive search for new Ni-free Ti-based SMAs, such as Ti–Nb–Ta and Ti–Nb–Zr, containing only biocompatible components [11–14]. In addition, these alloys exhibited low Young modulus (E) close to that of bone tissue, which is important for providing joint deformation of bones and implants.

Thermomechanical treatment of SMAs as developed in MISIS [15–17] normally includes: (a) cold (or warm) rolling/drawing to a true (logarithmic) strain of $e=0.3$ –2.0 and (b) subsequent post-deformation annealing at moderate temperatures (350–450 °C for Ti–Ni- and 550–600 °C for Ti–Nb-based alloys). In case of Ti–Ni, TMT can yield [18] either (i) polygonized “nanosubgrained” structure (hereinafter, nss) when $e=0.3$ –0.5; or (ii) mainly nanocrystalline structure (hereinafter, ns) when $e=1.5$ –2.0; or

* Corresponding author. Tel.: +7 495 638 4500; fax: +7 499 236 5298.
E-mail address: levashov@shs.misis.ru (E.A. Levashov).

Table 1
Materials used in experiments.

Substrate		Sample preparation procedure	Manufacturer
ms-Ti (Grade 4)	T1	Transversely cut	Dynamet Co
	T2	Longitudinally cut	Dynamet Co
ns-Ti (Conform)	T3	Transversely cut	NanoMet
	T4	Longitudinally cut	NanoMet
ms-Ti–50.9Ni	TN6	TMT: $e=0.47+700\text{ }^{\circ}\text{C}$ for 0.5 h+ $450\text{ }^{\circ}\text{C}$ for 1 h	MISIS
ns-Ti–50.7Ni	TN1	EPD: $e=1.6+450\text{ }^{\circ}\text{C}$ for 1 h	MISIS
nss-Ti–50.9Ni	TN4	TMT: $e=0.47+400\text{ }^{\circ}\text{C}$ for 1 h	MISIS
ms-Ti–Nb–Ta	TNT1	TMT: $e=0.37+750\text{ }^{\circ}\text{C}$ for 0.5 h	MISIS
nss-Ti–Nb–Ta	TNT2	TMT: $e=0.37+600\text{ }^{\circ}\text{C}$ for 1 h	
ms-Ti–Nb–Zr	TNZ1	TMT: $e=0.37+750\text{ }^{\circ}\text{C}$ for 0.5 h	MISIS
nss-Ti–Nb–Zr	TNZ2	TMT: $e=0.37+600\text{ }^{\circ}\text{C}$ for 0.5 h	

(iii) mixed nss–ns material when $e=0.5\text{--}1.5$. In case of Ti–Nb, TMT to any e and post-deformation annealing at $500\text{--}600\text{ }^{\circ}\text{C}$ result in formation of mainly nss–alloy [18].

The ns–Ti–Ni alloys exhibited ultimately high recovery stress and completely recoverable strain while the nss–ns alloys, ultimate fatigue resistance [15,16,19,20]. Ti–Nb-based SMAs with optimized nanosubgrained structure showed maximum fatigue resistance and the most perfect superelastic behavior [21].

Also note that Ti alloys are not biologically active, so that the surface of Ti implants is biologically inert. For the purpose of osteo-integration, it is desirable to cover the surface of implants with the so-called multicomponent biocompatible nanostructured films (MUBINAF) whose chemical, mechanical, tribological, and biological properties would allow their functioning in load-bearing implants [22–25].

At the same time, the data on the influence of inner structure of nanostructured titanium and its alloys (grain structure, dislocation structure, texture, and residual strain) on their mechanical properties (hardness H , Young modulus E , and elastic recovery R) are scarce in the literature. To our knowledge, systematic studies on the mechanical/tribological behavior of MUBINAFs deposited onto nanostructured Ti alloys by instrumented nanoindentation technique have not been conducted so far.

This paper aims at filling the above gap. We explored the mechanical properties of MUBINAFs deposited onto nanostructured Ti alloys and Ti-based shape memory alloys by instrumented indentation technique.

The current results were needed for validation of multiscale modeling results of indentation and localized deformation of nanostructured biomaterials aiming at elucidating a relationship between a deformation mechanism and mechanical behavior of MUBINAF/substrate systems.

2. Experimental

The materials used in the present study and sample preparation procedures are listed and characterized in Table 1.

3. Production of nanostructured Ti alloys and biocompatible coatings

3.1. Production of bulk nanostructured Ti-based materials

3.1.1. Equal-channel angular pressing by CONFORM scheme

Rods of Ti Grade 4 (12 mm in diameter, 500 mm long, from Dynamet Co., USA) were used as a starting material to produce nanostructured Ti (hereinafter ns-Ti). The rods were subjected to

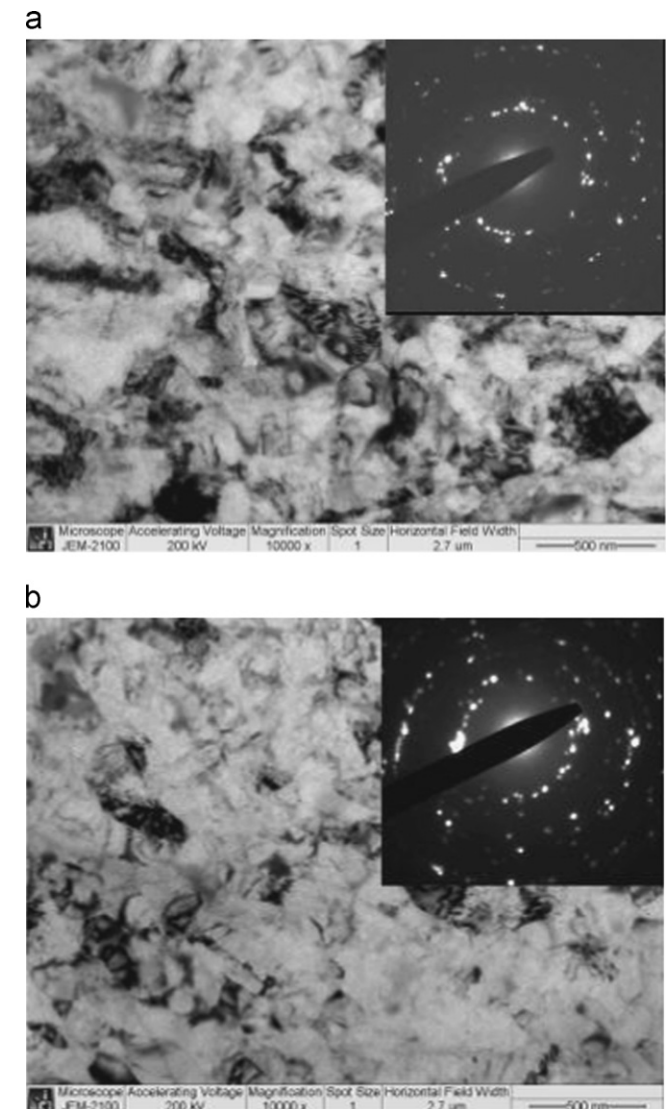


Fig. 1. Bright-field TEM images of Ti Grade 4 after ECAP-C processing ($n=6$): longitudinal (a) and transversal (b) sections.

6 passes of equal-channel angular pressing by CONFORM scheme (ECAP-C processing, [4,5]) in a die-set with 11×11 mm channels with the angle of channels intersection at 120° (which ensures strain accumulation $e=0.7$ per pass). Therefore, the ECAP-C treatment gave 11×11 mm square rods at the output.

3.1.2. Thermomechanical treatment

Nanostructured SMAs were prepared by TMT involving (1) cold plastic deformation (CPD) or electroplastic deformation (EPD) by rolling and (2) subsequent post-deformation annealing (PDA).

The plates of Ti–50.9% Ni alloy (4 mm thick) were quenched in water (after solution treatment at 800 °C, for 30 min) and then hot-rolled to a thickness of 2 mm. Thus prepared planks were cut into $2 \times 8 \times 100$ mm plates and rolled (DUO-210 rolling mill), in several passes, down to a thickness of 1.25 mm (10 mm wide). The accumulated true strain e was 0.47. Then the plates were cut into 14–16 mm-long samples, annealed at 400 °C for 1 h, and water-cooled. As a reference procedure, we used the following treatment: quenching at 700 °C, for 30 min + annealing (aging) at 450 °C, for 1 h; such a treatment yielded [15] the recrystallized, “coarse-grained” structure with the grain size $d_{gr} \approx 10 \mu\text{m}$.

The samples of nss-Ti–20.8Nb–5.5Zr and nss-Ti–19.7Nb–5.8Ta (at%) were prepared by cold rolling $2 \times 10 \times 150$ mm (Ti–Nb–Ta) and $2 \times 13 \times (20\text{--}100)$ mm blanks (Ti–Nb–Zr) to $e=0.37$ followed by annealing at 600 °C for 30 min (Ti–Nb–Zr) or for 1 h (Ti–Nb–Ta). Annealing at 750 °C for 30 min was used as a reference treatment yielding material with a grain size (d_{gr}) of around 30 μm [18].

3.1.3. Electroplastic deformation

The 2-mm thick plates of Ti–50.7% Ni alloy (analog of Ti–50.9% Ni alloy) fabricated by multiple hot rolling were cut into $2 \times 7 \times 200$ mm pieces and subjected to TMT, including EPD, in a DUO-120 rolling mill equipped with a generator of pulsed current. Rolling was carried out at a rate of 0.035 m/s under pulsed current ($f \approx 10^3 \text{ s}^{-1}$, $j=168 \text{ A/mm}^2$, $\tau=160 \mu\text{s}$) down to $e=1.6$ or 1.73. This was followed by annealing at 400 or 450 °C for 1 h and cutting into 15×9 mm-long samples. EPD was preceded by quenching at 700 °C.

3.2. Preparation of coatings

Multicomponent TiCaPCON coatings were deposited by magnetron sputtering combined with ion beam implantation at the initial stages using SHS-produced $\text{TiC}_{0.5}\text{--}10\% \text{ Ca}_3(\text{PO}_4)_2$ as a target [26,27] doped with alloying agents (added during preparation of green mixtures).

Prior to deposition, substrate plates were wet polished (about 0.2 mm deep) to R_a 10 nm using oxide suspension and hydrogen peroxide. The substrates were cleaned by isopropyl alcohol using ultrasonic bath. Then the substrates were warmed up to 250 °C and subjected to ion-beam etching to a depth of about 20 nm, after which R_a raised to 15–25 nm. During deposition, a distance from the target was 100 mm, pressure 0.1 Pa, magnetron current 2 A, and nitrogen content of gas 15%. The thickness of deposited coatings (as determined with a Wyko NT1100 profilometer) was 0.5–2.0 μm .

4. Instruments and methods

Tensile testing was carried out at room temperature by using an INSTRON machine (strain rate 10^{-3} s^{-1}) and cylindrical samples 15 mm long and 3 mm in diameter (according to GOST 1497-84). Small flat Ti samples ($4 \times 1.0 \times 0.25$ mm) were tested on a machine designed at USATU.

TEM images were taken with a JEM 2100 JEOL or Tesla BS-540 microscope. Metallographic samples were polished and acid-etched (4% HF, 20% HClO_4 , 76% H_2O).

The samples of ns-Ti for deposition of coatings were cut (in transversal and longitudinal directions) by electro-erosion

from the rods manufactured at NanoMet Ltd. (Table 1) as a half-finished material for implant applications ($d_{gr} \approx 150 \text{ nm}$, $\sigma = 1250 \text{ MPa}$).

Table 2
Tensile strength of starting and CONFORM-processed Ti (Grade 4).

State	Substrate	$\sigma_{0.2}$ (MPa)	UTS (MPa)	EI (%)	ψ (%)
Starting	T1, T2	625	760	24	50
Processed ($n=6$)	T3, T4	975	1020	13	54

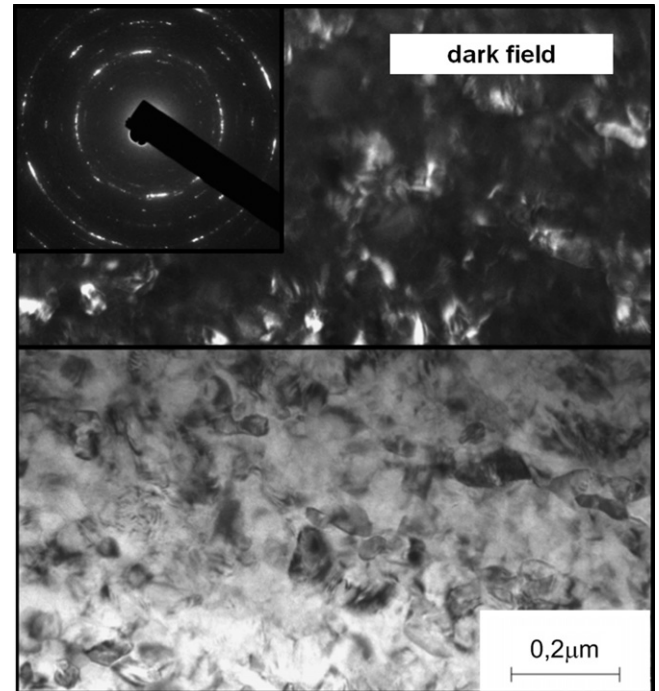


Fig. 2. Nanosubgrained structure of Ti–50.7% Ni alloy after TMT ($e=0.3+400$ °C for 1 h): dark-field image (upper), bright-field image (below), and diffraction pattern (inset).

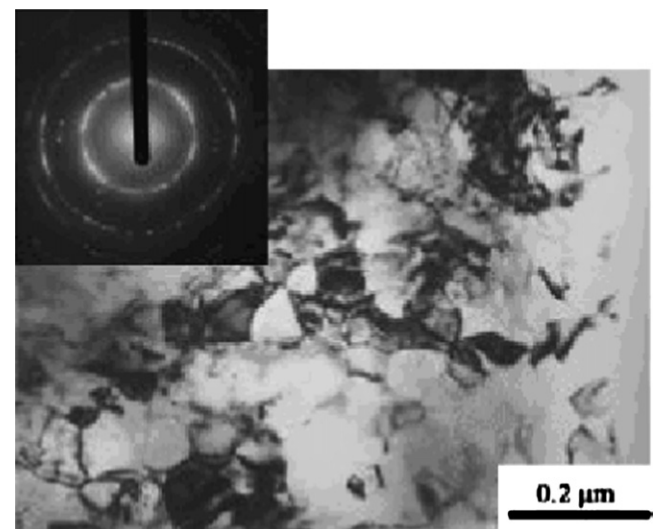


Fig. 3. Nanocrystalline structure of Ti–50.7% Ni alloy after EPD ($e=1.73+400$ °C for 1 h): dark-field image and diffraction pattern (inset).

Elemental composition of coatings was detected by optical emission spectroscopy of glowing discharge (Profiler 2 spectrometer, Horiba Jobin Yvon, France). Raman spectra were taken with a TRIAX spectrometer (Horiba Jobin Yvon, France) at a resolution of 4 cm^{-1} (λ_{ex} 514.5 nm). The coatings were also characterized by XPS (PHI 5500 Perkin-Elmer) and high-resolution TEM (JEM 2000EX, JEOL, Japan) at an accelerating voltage of 200 kV. The phase composition of samples was determined by means of X-ray diffraction (XRD). XRD patterns were recorded in the range of $10\text{--}90^\circ(2\theta)$ with spacing 0.1° and counting time of 9 s per each step in a “D8 Advance” (Bruker) diffractometer with a Cu $K\alpha$ radiation. In order to reduce the intensity of substrate peaks, the XRD analysis was performed in a glancing-beam mode under inclination of $3\text{--}5^\circ$.

Thin foils for studying the grain and subgrain structure of Ti–Ni alloys were prepared by electrolytic polishing in an electrolyte containing 10 ml HClO_4 and 90 ml CH_3COOH . Ti–Nb–Zr and Ti–Nb–Ta foils were prepared by jet electrolytic polishing in 15% solution of HNO_3 in ethanol using a TENUPO-5 device.

Tensile testing of Ti–Ni was performed as described in [16]. The results are given in Table 3. Multicycle mechanical testing of Ti–Nb–Zr samples was carried out in an MTS Minibionix machine using loading–unloading procedure [21].

Instrumented indentation experiments using a Berkovich diamond tip were performed at MISIS (NanoHardness Tester (NHT), CSM Instruments, Switzerland) as reported [28,29]. Since a maximal load was 2, 5, 10, 30, 100 or 250 mN, this allowed us to apply the Oliver–Pharr method in order to derive Young modulus E , hardness H [30], and elastic recovery R [31] at various penetration depths [32].

To study localized deformation [33], a series of Vickers indents were obtained using either a 402 MVD (Wolpert) or an NHT (CSM)

instrument. Such indents were then analyzed by optical (Axiovert CA25, Zeiss) and scanning electron microscopy (S-4800, Hitachi). A Scanning Probe microscope (NTEGRA, NT-MDT) was used for investigation of imprints obtained at 250 mN.

5. Results and discussion

5.1. Substrates of nanostructured Ti

Our metallographic data shown in Fig. 1 suggest that as-hot-rolled titanium exhibits a microstructure with the mean grain size of around $25\ \mu\text{m}$. After ECAP-C processing the size of grains/subgrains diminished down to 220 nm in longitudinal direction and to 180 nm in the transversal one (aspect ratio around 0.6). Dislocation density attained the value of $\rho \approx 10^{15}\ \text{m}^{-2}$.

After ECAP-C processing, the values of $\sigma_{0.2}$ and UTS grew by a factor of 1.5 (Table 2). The transversal strength is 10% higher as compared to the longitudinal one, which agrees with the literature data [2]. Although the relative elongation to failure (El) somewhat decreases (by 13%), the ductility of the material seems to be quite sufficient for implant applications.

5.2. Nanostructured shape memory alloys

Fig. 2 shows the structure of Ti–50.7% Ni alloy (analog of Ti–50.9% Ni) after TMT. The structure of B2-austenite consists of equiaxed elements 30–50 nm in size which form (in dark-field images) prolonged (0.2 μm and above) bright areas. Thus, there are mainly low-angle boundaries (sub-boundaries), and neighboring elements are subgrains (rather than grains). Hereinafter, such a

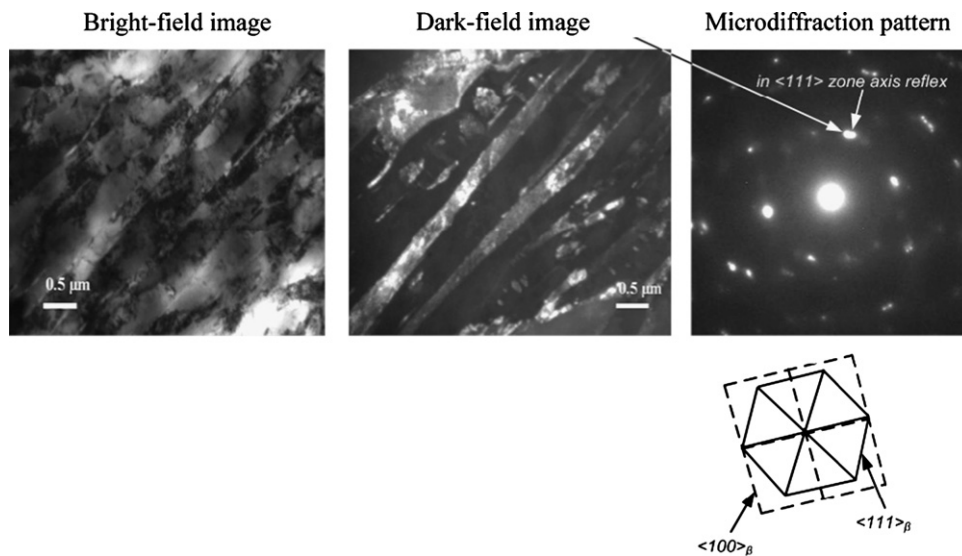


Fig. 4. Nanosubgrained structure and diffraction pattern of TN22 alloy (TMT: $e=0.37+600\text{ }^\circ\text{C}$ for 0.5 h).

Table 3

Strength parameters of Ti–50.7Ni alloy as determined at 255 K after TMT and reference processing [16].

e	Annealing temperature (K)	Structure	Transformation yield stress σ_{tr} (MPa)	Dislocation yield stress σ_y (MPa)	$\sigma_{\text{tr}} - \sigma_y$ (MPa)
0.3/1.7	973	ms, d_{gr} 10 μm	120/130	540/560	420/430
0.3	673	nss, d_{gr} 60 nm	110	1100	990
1.7	723	ns, d_{gr} 110 nm	220	1570	1350
	673	ns, d_{gr} 25 nm	290	1880	1590

structure will be referred to as nss (subgrain size σ_{sgr} below 100 nm). The diffraction pattern presented in Fig. 2 is typical of the so-called polygonized substructure with low-angle subgrain misorientations [15–17]. However, a certain number of individual reflections rarely distributed along diffraction rings indicates the presence of a limited quantity of high-angle misorientations as well.

Fig. 3 shows the structure of Ti–50.7% Ni alloy subjected to severe EPD ($e=1.73+400^\circ\text{C}$ for 1 h). In this case, the diffraction pattern is typical of a predominantly nanocrystalline structure (hereinafter, ns). Nevertheless, it cannot be discarded that some coarse grains have not been noticed during local TEM analysis [34].

Fig. 4 presents the nanosubgrained structure and diffraction pattern of **TNZZ** alloy. In this case, the diffraction pattern is indicative of the presence of the pure nss β -phase [35].

Table 3 presents the strength parameters of the Ti–50.7%Ni alloy as determined by tensile testing at 255 K after TMT and reference processing [16]. As follows from Table 3, a maximum value of dislocation yield stress, σ_y , is exhibited by ns-materials while medium values, by nss-materials; both exceeding a level reached in reference processing. Similar behavior was observed for the difference between σ_y and transformation yield stress, σ_{tr} , and hence between the resources of maximum recovery stresses and completely recoverable strains [16].

For Ti–Nb–Zr and Ti–Nb–Ta alloys, typical is imperfect super-elastic behavior in the first cycle of room-temperature loading–unloading tests [21]. In this case, an optimized nss exhibits a markedly lower residual strain and a higher fatigue resistance compared to a recrystallized one.

5.3. Structure of bioactive coatings

According to the scanning electron microscopy data the TiCaPCON coating have a dense and uniform structure. XRD data suggest that this is largely the *fcc* TiCN with $a=0.429$ nm and a crystallite size (L) of 4–5 nm (as estimated using the Debye–Scherrer formula). The Raman spectrum (Fig. 5a) exhibits two peaks (below 750 cm^{-1}) that can be assigned to TiC [36]. A broad band at $1200\text{--}1700\text{ cm}^{-1}$ can be attributed to diamond-like carbon [24,25]. The element depth profiles indicate also the presence of O(12.8 at. %), Ca(2.1 at. %), and P (0.6 at%).

Previously, we have reported [25] that such coatings also contain amorphous TiO_x and CaO (on grain boundaries) in addition to P–O and C–O bonds. This is in line with Fig. 5b showing a high-definition micrograph of TiCaPCON coating. A crystallite with $L=5\text{--}10$ nm is seen to be surrounded by a diffraction-silent amorphous layer.

5.4. Instrumented indentation

5.4.1. Mechanical properties of substrates as a function of penetration depth

Fig. 6 shows the indentation curves for the samples of **T1** and **TN4** taken at $P=5, 10, 30,$ and 100 mN. The loading curves in Fig. 6a and b are seen to be nearly coincident for various loads, which is indicative of in-depth uniformity of both the materials. At equal P , the depths of penetration into **T1** and **TN4** are close, which indicates their close hardness, but the area between the load–unload curves is markedly smaller in case of **TN4**. The latter can be related to accumulation of reversible deformation in the near-surface layers due to strain-induced transformation (partial pseudo-elasticity). The values of E and R (correlating with the slope of unloading curves) are also different: in case of **T1**, the E values are greater while the values of R , lower.

Fig. 7 shows the mechanical properties of **T1**, **T3**, **TN4**, and **TNZZ** substrates as inferred from indentation experiments.

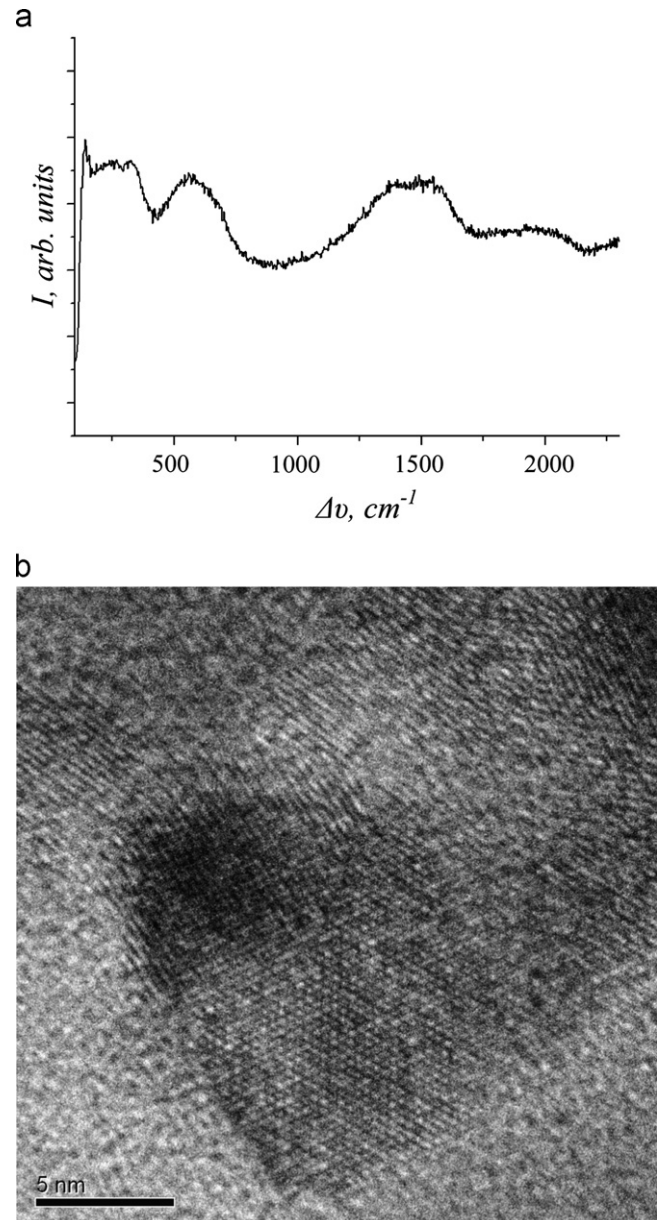


Fig. 5. Raman spectrum (a) and high resolution TEM micrograph (b) of TiCaPCON coating.

The highest H (above 5 GPa) and E (about 140 GPa) values were shown by nanostructured **T3**. For micro-structured **T1**, these magnitudes are lower by 25% and 13%, respectively. The R values (for loads < 100 mN) are below 12% and 17% for **T1** and **T3**, respectively. On the contrary, a 10–13% decrease in the E values of nanostructured materials was detected [2] by acoustic measurements.

The lowest H values (below 2 GPa) were exhibited by nss-Ti–Nb–Zr alloy (**TNZZ**) while the lowest E (below 60 GPa), by **TN4**. For Ti–Nb based alloys, $E=60\text{--}77$ GPa alloys.

For **TN4**, $R > 40\%$, although both Ti–Nb alloys show the same R as ns-Ti (**T3**). This seems reasonable because the crystallographic resource of recoverable strain Ti–Nb–Ta is known [37,38] to be lower than that for Ti–Ni: 3 and 10.5%, respectively. Moreover, the hardness of Ti–Nb alloys is lower than that of Ti–Ni. The above factors explain a lower contribution from reversible deformation into the indentation behavior of shape memory alloys based on Ti–Nb.

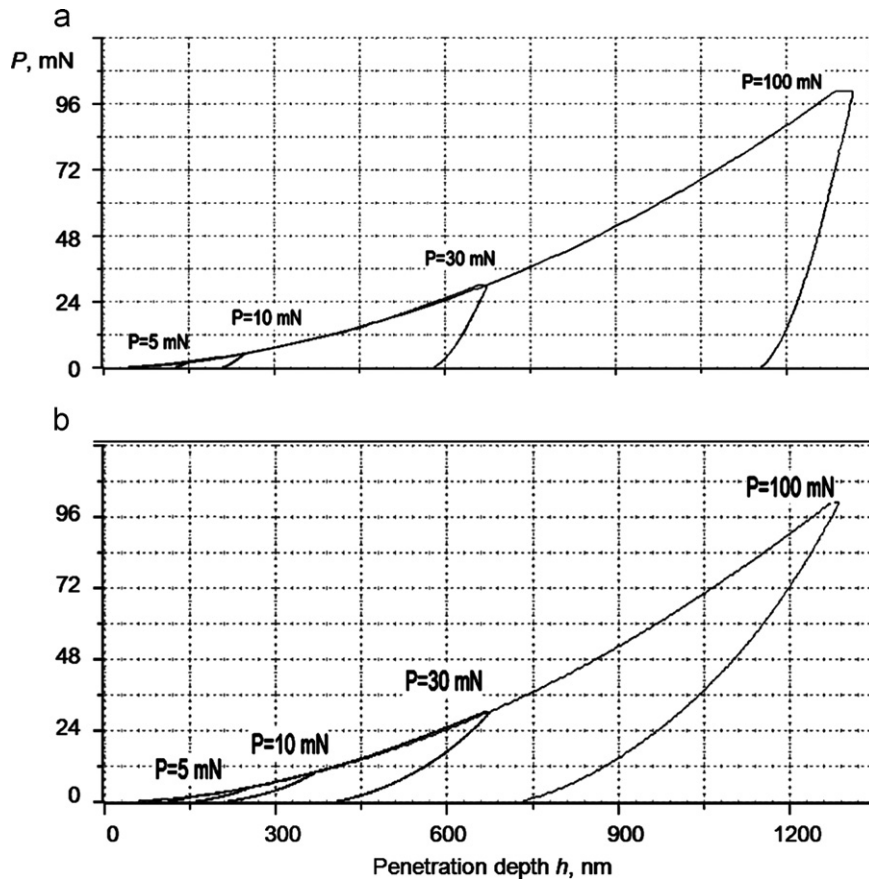


Fig. 6. Indentation curves for the samples of (a) microstructured titanium T1 and (b) nanostructured shape memory alloy TN4 as taken at different loads $P=5$, 10, 30, and 100 mN.

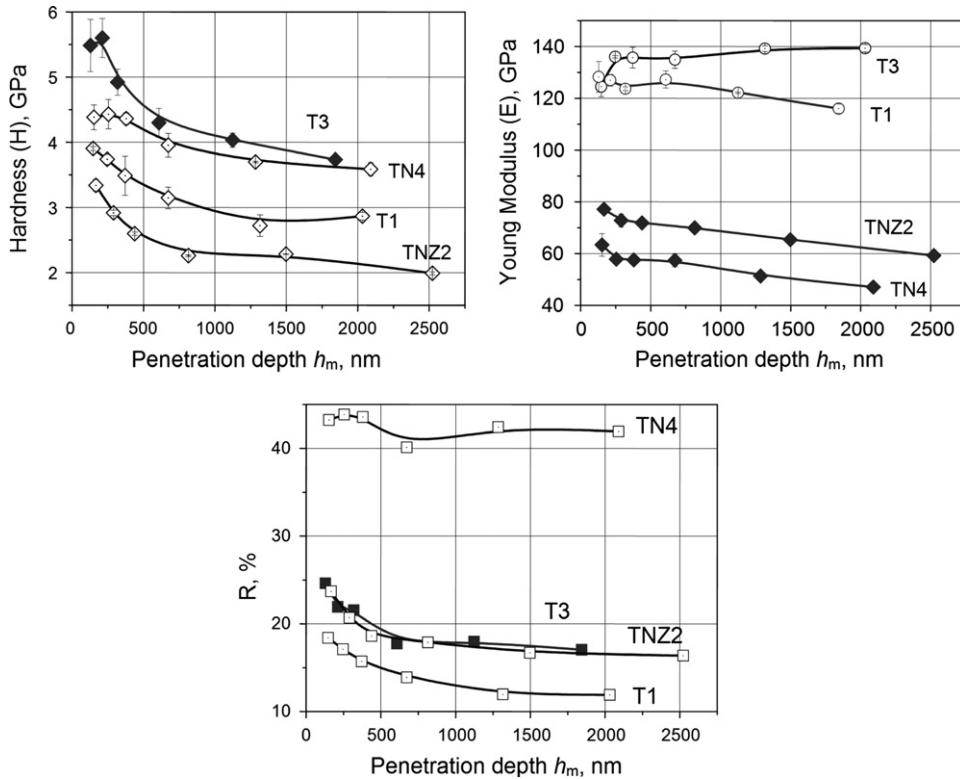


Fig. 7. Mechanical properties of substrates as obtained by instrumented indentation: microstructured titanium (T1), nanostructured titanium (T3), nanostructured shape memory alloy (TN4), and nanostructured TiNbZr alloy (TNZ2).

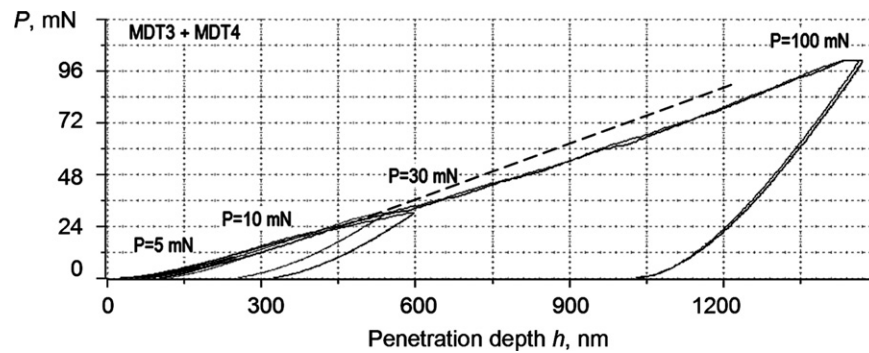


Fig. 8. Indentation curves for the coatings deposited onto transverse cross-section (MD T3) and longitudinal cross-section (MD T4) of substrates cut of nanostructured titanium rod. The figure illustrates a decline in the curve slopes within the range of $P=10\text{--}30$ mN due to sinking-in of the substrate.

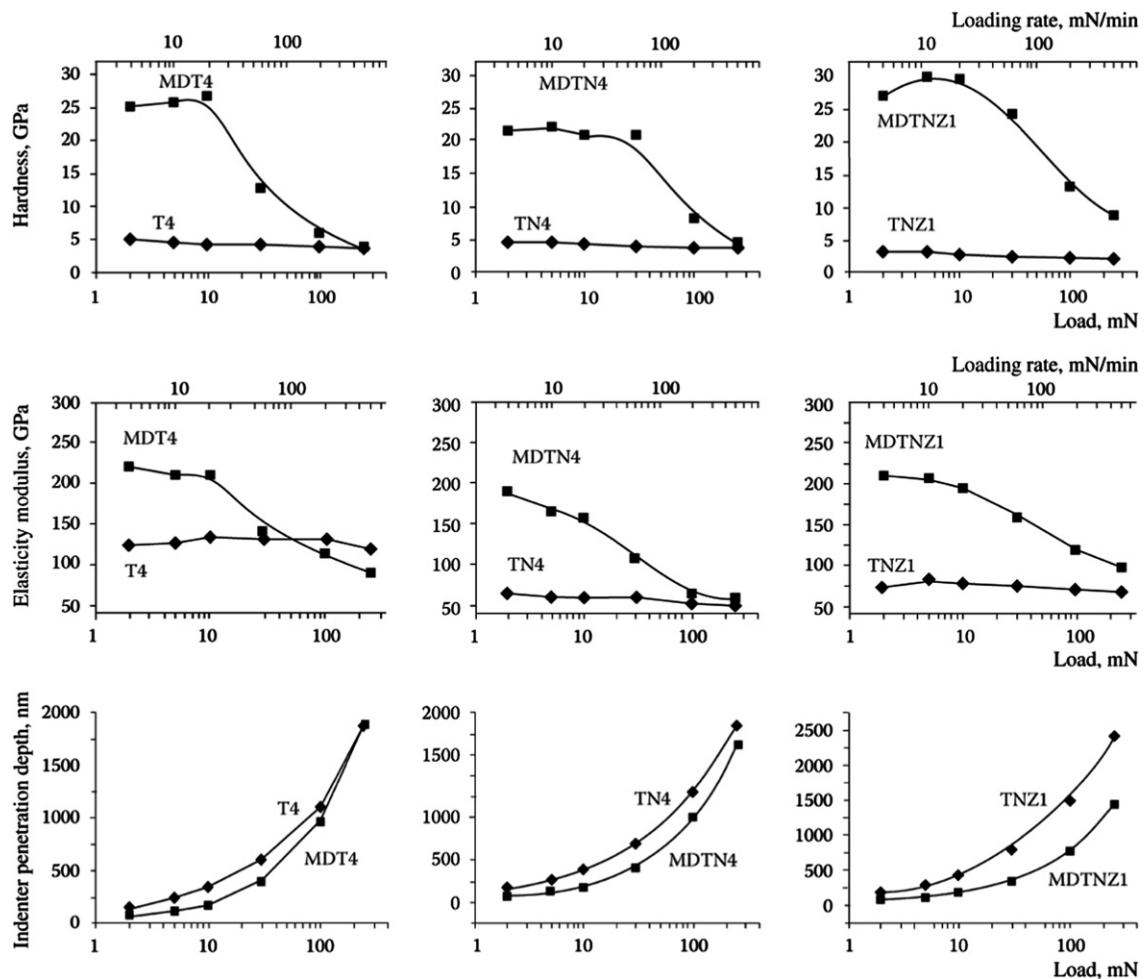


Fig. 9. Hardness H , Young modulus E , and maximum penetration depth h_m as a function of applied load P and loading rate for the coatings (indicated) deposited onto ns-Ti, ns-TiNi, and ns-TiNbZr substrates.

5.4.2. Mechanical properties of coating–substrate systems as a function of penetration depth

Deposition of biocompatible coatings onto all substrates (listed in Table 1) was found to improve the mechanical properties of the surface, especially at low loads. As is seen in Fig. 8, the slope of loading curves changes with increasing P . This can be explained by a play between indentation of (1) a harder and higher- E coating ($E=200$ GPa) and (2) a softer and lower- E substrate (140 GPa for ns-Ti, 120 GPa for ms-Ti, and <70 GPa for shape memory alloys).

With increasing P , the values of H , E , and R gradually decreased down to the magnitudes typical of substrate material (Fig. 9).

5.4.3. Effect of ECAP-C processing direction

Indentation results exhibited little or no dependence on whether the samples were cut alongside or across the direction of drawing. As is seen in Fig. 8, the indentation curves for MD T3 and MD T4 can be regarded as coincident (here and hereinafter MD stands for ‘magnetron deposited’).

5.4.4. Effect of substrate type

Fig. 9 shows hardness H , Young's modulus E , and maximum penetration depth h_m as a function of applied load P and load rate \dot{P} for the coatings (indicated) deposited onto ns-Ti, ns-TiNi, and ns-TiNbZr substrates. These results can be used to follow up the dependence of mechanical properties of coatings on the elastic properties of substrate. It has been found that the coatings deposited into ms-Ti and ns-Ti showed 10% higher values of E as compared to those deposited onto low- E shape memory alloys. The situation gets reversed in case of TiNi substrates with $E < 65$ GPa. It comes out that the low E values of deposited coatings correlate with the lowest E values of substrate.

5.5. Mechanism of localized deformation

All types of uncoated samples showed the homogeneous deformation at indentation as one can see at SEM images of indents on the surface of **T1** and **TN4** presented in Fig. 10. The indents are seen to be well discernible on the polished surface of the above substrates.

As is known [39], deformation of nanostructured coatings can proceed in two modes: (a) by the so-called homogeneous mechanism (in case of weak chemical bonding between structural units) and (b) inhomogeneous mechanism involving the formation of shear strips (in case of strong chemical bonding between structural units). It was also suggested [40] to characterize a resistance of material to plastic deformation by

parameter H^3/E^2 . Ceramic coatings with $H^3/E^2 > 0.6$ deformed by mechanism (a) while those with $H^3/E^2 < 0.5$, by mechanism (b). The smaller H^3/E^2 , the lower threshold P value for appearance of shear strips.

As can be assessed from the data in Fig. 9, for the TiCaPCON/substrate system parameter H^3/E^2 can be varied from 0.32 (TiNi) to 0.4 (Ti) and to 0.55 (TiNbZr). So one could expect the formation of slide steps on the surface of indents, which has been observed in some experiments. Indents on MUBINAF are less discernible because of higher surface roughness and elastic recovery at low P . In the process of ion beam etching, the surface roughness increases, because the material grains oriented at different angles with respect to incident ion beam are etched at different rates. As a result, surface roughness becomes comparable with the depth of indents obtained for $P < 250$ mN. For this reason, all experiments of this kind (Figs. 11–14) were conducted for $P \geq 250$ mN.

As follows from Fig. 11, for **MD T1** and **MD T3** the indents exhibit a system of the steps parallel to indent faces. An increase in P led to cracking (arrow in Fig. 11).

Under low loads (250 mN), the steps are seen to appear over the entire indent area (Fig. 11). Under high loads (1000 mN), the steps formed only near the indent faces. With increasing depth h , the steps become less notable or disappear altogether. This is because penetration depth h becomes larger than coating thickness d . For instance, at $d = 1.5$ μm and $P = 500$ and 1000 mN, the h values were 2.3 and 3.5 μm , respectively (**MD T1**) and 2.1 and 3.3 μm (**MD T3**), respectively.

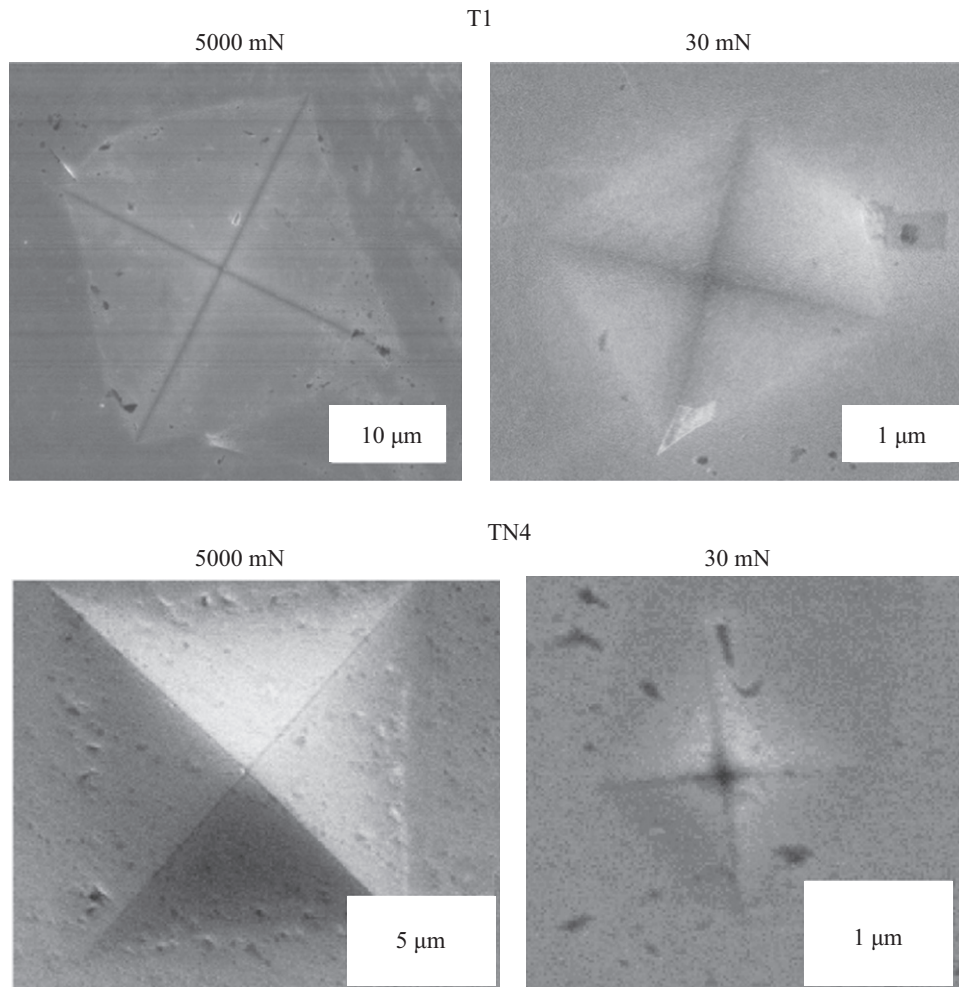


Fig. 10. SEM images of indents on the surface of ms-Ti (**T1**) and ns-TiNi (**TN4**) at the applied load 30 and 5000 mN.

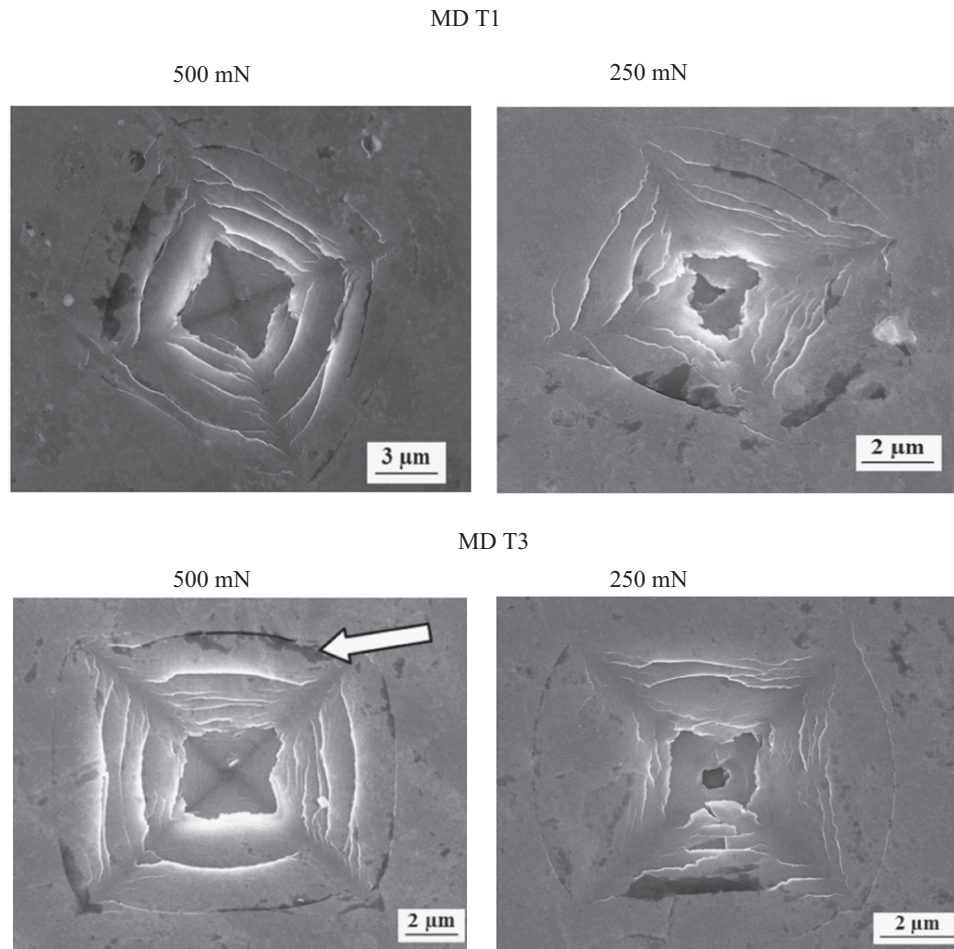


Fig. 11. SEM images of indents on the coated surface of ms-Ti (**MD T1**) and ns-Ti (**MD T3**) at the applied load 250 and 500 mN.

The SEM images of indents on the coated surface of ns-TiNi and ms-TiNi (Fig. 12) show some traces of inhomogeneous deformation at loads $P \geq 250$ mN, but they are not so notable as at ms-Ti and ns-Ti (Fig. 11).

The traces of inhomogeneous deformation for coated ms-TiNbTa and ns-TiNbTa become discernible for $P=500-5000$ mN. In case of ms-TiNbTa substrate, inhomogeneous deformation manifests itself over the entire range of P (Fig. 13).

Fig. 14 shows the SPM image of indent, one of that shown on Fig. 11, obtained on the **MD T3** (TiCaPCON/ns-Ti system) at of 250 mN. The mean width of shear bands (terraces) is 0.1–0.2 μm , in agreement with [40]. In case of the coatings deposited on SMA substrates (TiNi, Fig. 12 and TiNb-based, Fig. 13), the appearance of shear strips is less pronounced. It may be connected with pseudo elastic recovery of the SMA substrates compared to that made of micro and nanostructured titanium. In fact the depth of imprint is about twice less for shape memory substrates (**MD TNT2**, curve 'c') than for ns-Ti (**MD T3**, curve 'b') as can be seen at Fig. 15. It should be noted also that steps on the profile are larger at **MD T3** system and more fine for **MD TNT2** one. Anyhow both the profiles differ from one received for uncoated ms-Ti (**T1**, curve 'a').

It can therefore be concluded that deposition of TiCaPCON coating not only improves the mechanical properties (hardness, Young modulus, elastic recovery) but also changes a mechanism of localized deformation in the near-surface layers. Deformation was found to proceed inhomogeneous, through formation of shear bands during penetration of a Vickers diamond indenter

into coatings/substrate system. Formation of shear strips is most pronounced in case of substrates with higher E and lower elastic recovery (R), such as ms-Ti ($E=125-130$ GPa, $R=10-12\%$).

6. Conclusions

- (1) Instrumented indentation in conditions of localized deformation was used to characterize the mechanical properties of biocompatible nanostructured titanium alloys and of the TiCaPCON multicomponent bioactive ns-films (MUBINAF) deposited on their surface.
- (2) For shape memory alloys (SMAs), the surface area between the load–unload curves is markedly lower while the elastic recovery, higher as compared to those for ms-Ti and ns-Ti. The effect was associated with predominance of accumulated reversible deformation due to shear (martensite-type) strain-induced transformation in the near-surface layer.
- (3) The highest values of H (above 5 GPa) and E (around 140 GPa) are exhibited by ns-Ti. For ms-Ti, the above magnitudes are lower by 25% and 13%, respectively. Elastic recovery R does not exceed 12% for ms-Ti and has a value of 17% for ns-Ti (for $P > 100$ mN).
- (4) The lowest hardness (< 2 GPa) was exhibited by nanostructured Ti–Nb-based SMA, while the lowest E value (< 60 GPa) was found for nanostructured TiNi-based SMA. For SMAs

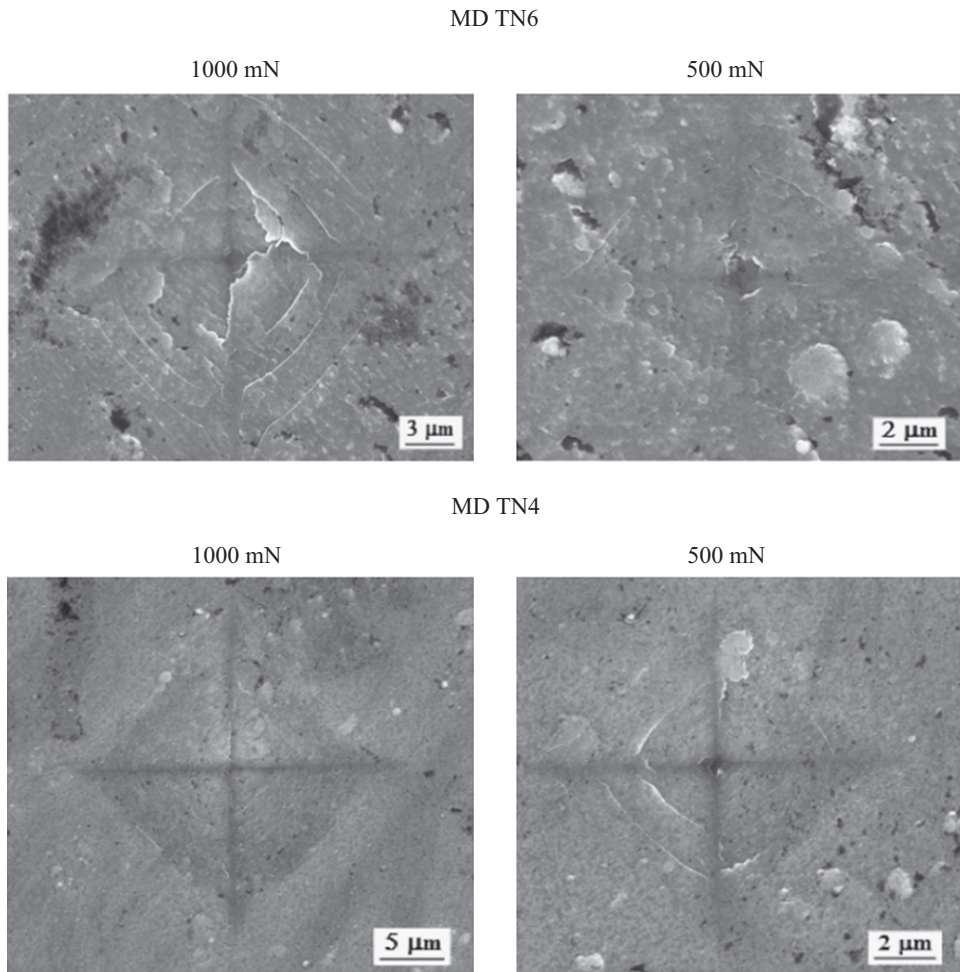


Fig. 12. SEM images of indents on the coated surface of ms-TiNi (**MD TN6**) and ns-TiNi (**MD TN4**) at the applied load 500 and 1000 mN.

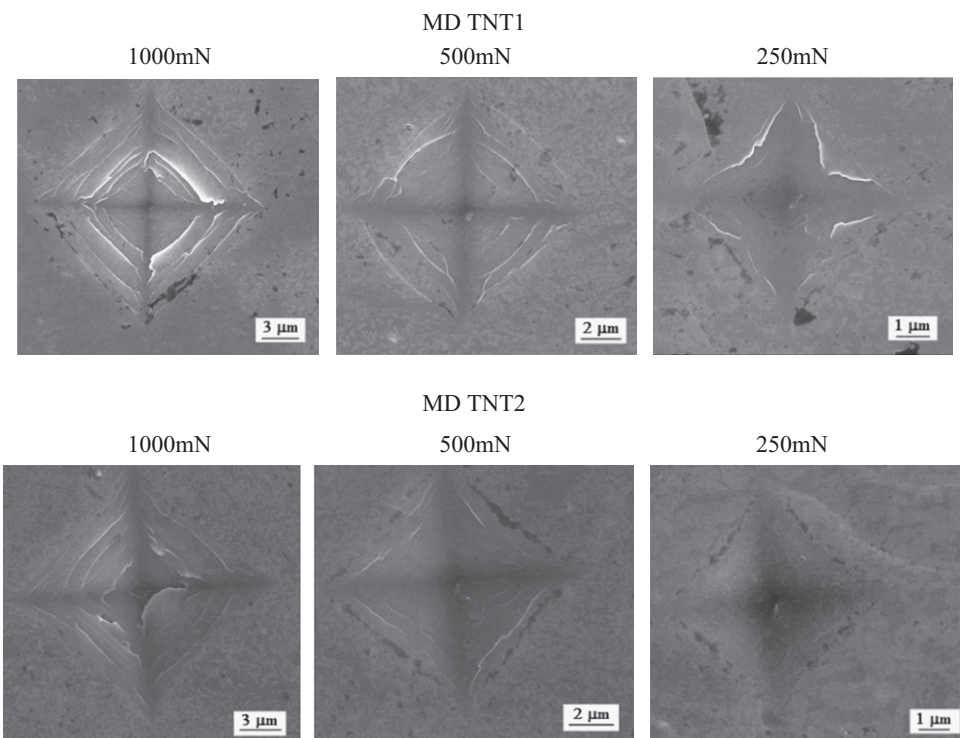


Fig. 13. SEM images of indents on the coated surface of ms-TiNbTa (**MD TNT1**) and ns-TiNbTa (**MD TNT2**) at the applied load 250, 500, and 1000 mN.

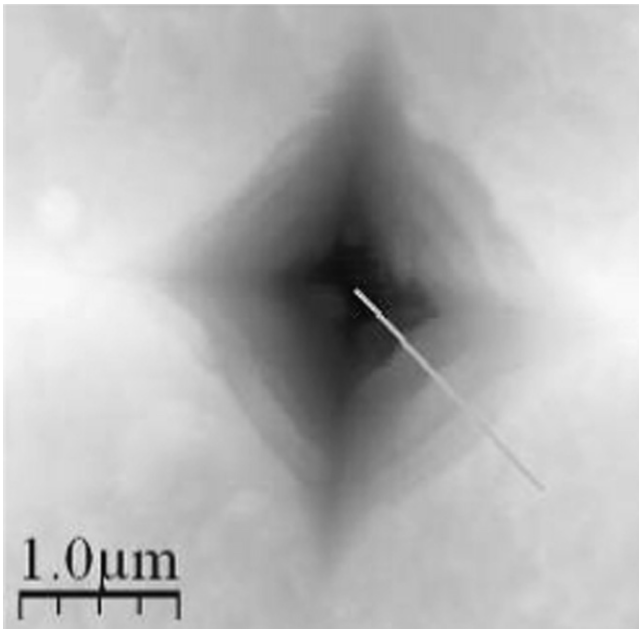


Fig. 14. Scanning Probe Microscopy (SPM) image of indent on the 'TiCaPCON/ns-Ti (MDT3)' system ($P=250$ mN).

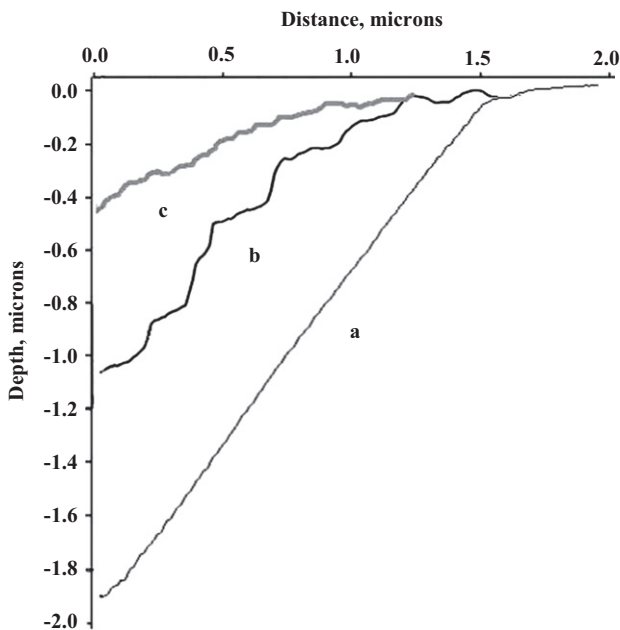


Fig. 15. Physical profile of the indents ($P=250$ mN) for ms-Ti (T1) (a) and for systems: 'TiCaPCON/ns-Ti (MDT3)' (b) and 'TiCaPCON/ns-TiNbTa (MDTNT2)' (c).

based on Ti–Nb, $E=60\text{--}77$ GPa. For TiNi, R is somewhat higher ($>40\%$), although both TiNb-based SMAs exhibit $R=16\text{--}17\%$.

- (5) The mechanical properties of ms-Ti and ns-Ti samples cut across and along the direction of drawing were found (within measurement accuracy) to be the same. The properties of deposited coatings are independent of the orientation of substrate surface.
- (6) In contrast to bulk materials, localized deformation of TiCaPCON coatings proceeds by the mechanism of inhomogeneous deformation involving the formation of shear bands. Formation of the bands is more pronounced in case of coatings with higher E and lower R , such as ms-Ti ($E=125\text{--}130$ GPa, $R=10\text{--}12\%$).

Acknowledgments

This work was carried out in the framework of the ViNaT Project, Contract no. 295322, FP7-NMP-2011-EU-Russia, NMP.2011.1.4-5 coordinated with State Contract no. 16.523.12.3002 from the Russian Ministry of Education and Science on the Federal Targeted Program Research and Development under Priority Directions of Scientific-Technological Complex of Russia for 2007–2013.

References

- [1] D.M. Brunette, P. Tengvall, M. Textor, P. Thomsen, Titanium in Medicine, Springer, Berlin, 2001.
- [2] I.V. Aleksandrov, Ob"emnye nanostrukturnye metallicheskie materialy: Poluchenie, struktura i svoystva (Bulk Nanostructured Metallic Materials: Preparation, Structure, and Properties), Akademkniga, Moscow, 2007.
- [3] R.Z. Valiev, I.P. Semenova, V.V. Latysh, A.V. Shchherbakov, E.B. Yakushina, Ross. Nanotekhnol. 3 (2008) 45–56.
- [4] G.I. Raab, R.Z. Valiev, D.V. Gunderov, T. Lowe, A. Misra, Yu. Zhu, Mater. Sci. Forum 584–586 (2008) 80–88.
- [5] G.I. Raab, A.V. Polyakov, D.V. Gunderov, R.Z. Valiev, Metally 5 (2009) 57–62.
- [6] T.W. Duerig, K.N. Melton, D. Stockel, C.M. Wayman (Eds.), Engineering Aspects of Shape Memory Alloys, Butterworth–Heinemann, London, 1990.
- [7] K. Otsuka, C.M. Wayman (Eds.), Shape Memory Materials, Cambridge University Press, Cambridge, 1999.
- [8] S. Brailovski, V. Prokoshkin, F. Terriault, P. Trochu (Eds.), Shape Memory Alloys: Fundamentals, Modeling and Applications, ETS Publ., Montreal, 2003.
- [9] L.A. Monasevich (Ed.), Effekty pamyati formy i ikh primenenie v meditsinske (Shape Memory Effect and Its Medical Applications), Nauka, Novosibirsk, 1992.
- [10] V.G. Pushin (Ed.), Splavy nikelida titana s pamyat'yu formy (Titanium Nickelide Alloys with Shape Memory). Part I, Izd. Ural Otd. RAN, Yekaterinburg, 2006.
- [11] M.I. Petrzhik, S.G. Fedotov, Thermal stability and dynamics of martensitic structure in Ti–(Ta,Nb) alloys, Proceedings of XVI Conference on Applied Crystallography, World Scientific Publishing, Cieszyn, Poland, 1995, pp. 273–276.
- [12] J.I. Kim, H.Y. Kim, T. Inamura, H. Hosoda, S. Miyazaki, Mater. Sci. Eng. A 403 (2005) 334–339.
- [13] H.Y. Kim, T. Sasaki, K. Okutsu, J.I. Kim, T. Inamura, H. Hosoda, S. Miyazaki, Acta Mater. 54 (2006) 423–433.
- [14] T. Yoneyama, S. Miyazaki, Shape Memory Alloys for Biomedical Applications, Woodhead Publishing, London, 2010.
- [15] V. Brailovski, S.D. Prokoshkin, I.Yu. Khmelevskaya, K.E. Inaekyan, V. Demers, S.V. Dobatkin, E.V. Tatyannin, Mater. Trans. 47 (2006) 795–804.
- [16] S.D. Prokoshkin, V. Brailovski, K.E. Inaekyan, V. Demers, I.Yu. Khmelevskaya, S.V. Dobatkin, E.V. Tatyannin, Mater. Sci. Eng. A 481–482 (2008) 114–118.
- [17] S.D. Prokoshkin, V. Brailovski, A.V. Korotitskiy, K.E. Inaekyan, A.M. Glezer, Phys. Met. Metallogr. 110 (2010) 289–303.
- [18] S.M. Dubinskiy, S.D. Prokoshkin, V. Brailovski, A.V. Korotitskiy, K.E. Inaekyan, M.R. Filonov, M.I. Petrzhik, Phys. Met. Metallogr. 112 (2011) 529–542.
- [19] V. Demers, V. Brailovski, S. Prokoshkin, K. Inaekyan, Mater. Sci. Eng. A 513–514 (2009) 185–196.
- [20] V. Brailovski, S. Prokoshkin, K. Inaekyan, V. Demers, J. Alloys Compd. 509 (2011) 2066–2075.
- [21] V. Brailovski, S. Prokoshkin, K. Inaekyan, S. Dubinskiy, M. Gauthier, Mater. Sci. Forum 706–709 (2012) 455–460.
- [22] D.V. Shtansky, A.S. Grigoryan, A.K. Toporkova, A.N. Sheveiko, F.V. Kiryukhantsev-Korneev, Surf. Coat. Technol. 206 (2011) 1188–1195.
- [23] D.V. Shtansky, N.A. Gloushankova, A.N. Sheveiko, F.V. Kiryukhantsev-Korneev, I.A. Bashkova, B.N. Mavrin, S.G. Ignatov, S.Yu. Filipovich, C. Rojas, Surf. Coat. Technol. 205 (2010) 728–739.
- [24] D.V. Shtansky, N.A. Gloushankova, I.A. Bashkova, M.A. Kharitonova, T.G. Moizhess, A.N. Sheveiko, F.V. Kiryukhantsev-Korneev, A. Osaka, B.N. Mavrin, E.A. Levashov, Surf. Coat. Technol. 202 (2008) 3615–3624.
- [25] D.V. Shtansky, N.A. Gloushankova, I.A. Bashkova, M.I. Petrzhik, A.N. Sheveiko, F.V. Kiryukhantsev-Korneev, I.V. Reshetov, A.S. Grigoryan, E.A. Levashov, Surf. Coat. Technol. 201 (2006) 4111–4118.
- [26] E.A. Levashov, S. Pogozhev, V.V. Kurbatkina, Advanced ceramic target materials produced by self-propagating high-temperature synthesis for deposition of functional nanostructured coatings, in: C. Sikalidis (Ed.), Advances in Ceramics—Synthesis and Characterization: Processing and Specific Application, InTech, Rijeka, Croatia, 2011, pp. 2–48.
- [27] E.A. Levashov, A.S. Rogachev, V.V. Kurbatkina, M. Maksimov, V.I. Yuhvid, Perspektivnyye materialy i tekhnologii samorasprostranyayushchegosya vysokotemperaturnogo sinteza: Uchebnoe posobie (Promissory Materials and Processes of Self-Propagating High-Temperature Synthesis: A Tutorial), Izd. MISIS, Moscow, 2011.
- [28] M.I. Petrzhik, E.A. Levashov, Crystallogr. Rep. 52 (2007) 966–974.
- [29] E.A. Levashov, M.I. Petrzhik, M.Ya. Tyurina, F.V. Kiryukhantsev-Korneev, P.A. Tsygankov, A.S. Rogachev, Metallurgist 54 (9–10) (2011) 623–634.
- [30] W.C. Oliver, G.M. Pharr, J. Mater. Res. 7 (1992) 1564–1583.

- [31] J. Musil, F. Kunc, H. Zeman, H. Polakova, *Surf. Coat. Technol.* 154 (2002) 304–313.
- [32] V. Milman, A.A. Golubenko, S.N. Dub, *Acta Mater.* 59 (2011) 7480–7487.
- [33] R.A. Andrievski, G.V. Kalinnikov, J. Jauberteau, J. Bates, *J. Mater. Sci.* 35 (2000) 2799–2806.
- [34] S.D. Prokoshkin, V.V. Stolyarov, A.V. Korotitskiy, K.E. Inaekyan, E.S. Danilov, I.Yu. Khmelevskaya, A.M. Glezer, S.M. Makushev, U.Kh. Ugurchiev, *Phys. Met. Metallogr.* 108 (2009) 619–624.
- [35] S. Prokoshkin, V. Brailovski, K. Inaekyan, A. Korotitskiy, S. Dubinskiy, M. Filonov, M. Petrzhih, *Mater. Sci. Forum* 706–709 (2012) 1931–1936.
- [36] B.H. Lohse, A. Calka, J. Alloys Compd. 434–435 (2007) 405–409.
- [37] S. Zhukova, M.I. Petrzhih, S.D. Prokoshkin, *Metally* (6) (2010) 77–84.
- [38] S.D. Prokoshkin, A.V. Korotitskiy, V. Brailovski, K.E. Inaekyan, S.M. Dubinskiy, *Phys. Met. Metallogr.* 112 (2011) 170–187.
- [39] R.A. Andrievski, G.V. Kalinnikov, *Surf. Coat. Technol.* 142–144 (2001) 573–581.
- [40] D.V. Shtansky, S.A. Kulinich, E.A. Levashov, A.N. Sheveiko, F.V. Kiriuhancev, J.J. Moore, *Thin Solid Films* 420–421 (2002) 330–337.